IEEE Access
Multidisciplinary | Rapid Review | Open Access Journal

Received August 2, 2019, accepted August 30, 2019, date of publication September 9, 2019, date of current version September 25, 2019.

Digital Object Identifier 10.1109/ACCESS.2019.2939784

Computational Depth Imaging Using the Fast Deconvolution Method

SHEN SHANSHAN[1,2], CHEN QIAN[1], HE WEI JI[1], AND GU GUO HUA[1]

[1]Jiangsu Key Laboratory of Spectral Imaging and Intelligence Sense (SIIS), Nanjing University of Science and Technology, Nanjing 210094, China
[2]College of Zijin, Nanjing University of Science and Technology, Nanjing 210023, China

Corresponding author: Chen Qian (chenqian@njust.edu.cn)

This work was supported in part by the Seventh Six-talent Peak Project of Jiangsu Province under Grant 2014-DZXX-007, in part by the National Natural Science Foundation of China under Grant 61271332 and Grant 61875088, in part by the Fundamental Research Funds for the Central Universities under Grant 30920140112012, and in part by the Blue project of Jiangsu Province under Grant QL016.

ABSTRACT Pseudo-random spread spectrum photon counting (PSSPC) is a well-established technique for three-dimensional (3D) imaging. Based on the pseudo-random spread spectrum photon counting system, a fast imaging technique that is able to accurately recover multiple depths at individual pixels is presented. Firstly, a pre-filtering algorithm is used to denoise the original data. Then the accelerated Richardson–Lucy iterative deconvolution algorithm is introduced. The method is based on the principles of vector extrapolation and does not require the minimization of a cost function. For multi-depth estimation in the presence of moderate background light, we experimentally demonstrate that our imaging technique outperforms the existing method. We have successfully improved the range resolution from 21cm to 8cm, thus breaking the Full Width at Half-Maximum (FWHM) resolution limit. The separation Root Mean Square Error (RMSE) has been reduced to 3.82cm by the proposed method for the surface-to-surface separation of 8cm. This is a factor of 4 improvement over the conventional method for multi-depth recovery. Also, our imager has achieved 0.5cm lateral resolution by distinguishing two squares closely placed 0.5cm apart from each other.

INDEX TERMS Pseudo-random spread spectrum photon counting, deconvolution, accelerated Richardson–Lucy, separation RMSE.

I. INTRODUCTION

The Pseudo-random Spread Spectrum Photon Counting (PSSPC) is the combination of two popular and well-established techniques, namely the Time Correlated Photon Counting technique and the Pseudo-random Spread Spectrum technique [1]–[4]. This technique has the ability to acquire three-dimensional (3D) structure of a scene in many applications, such as biometrics [1] and TOF cameras [2], [3]. Shen *et al.* [5] demonstrated that the 2.5GHz random pattern bit-stream was well suited for implementation in the one-dimensional time-of-flight ranging system and the range error due to different echo energy was calibrated. The PSSPC technique indeed has some unique benefits compared to other techniques such as phase shifting, heterodyne, and frequency modulated imaging technique [6]. These benefits involve long unambiguous range, the ability to resolve multiple targets and low mutual interference between devices. For example, instead of the sinusoidal modulation method, applying the PSSPC to the TOF camera solved the range aliasing problem. B. Buttgen *et al.* [2] employed eight such cameras to enhance the range resolution to 12cm at a range of 7.5 meter. The range resolution is determined by a pseudo-random binary sequence (PRBS) bit width [7]–[9]. For instance, a bit width of 0.4ns would normally produce a system with a resolution limited to 6cm under high signal-to-noise ratio (SNR) assumption and long enough integration time regardless of systematic transient distortions, if not, this resolution can be reduced by orders of magnitude. Besides, objects have complex patterns of light being reflected at different depths even at a single pixel shown in Fig.1. Each example of scene indicates that one surface return signal (the blue dashed line) and the other surface return signal (the orange dashed line) are collected by the detector shown in Fig.1 (a) and (b). Then the range profiles are calculated shown in Fig.1(c). As the surface-to-surface separation of the squares from the flat board in Fig.1(a) or the gap between the two squares is small in Fig.1(b), one of the reflections is obscure (red circle) shown in Fig.1(c). We fail to distinguish the two depths estimated from the one-dimensional

The associate editor coordinating the review of this manuscript and approving it for publication was Huaqing Li.

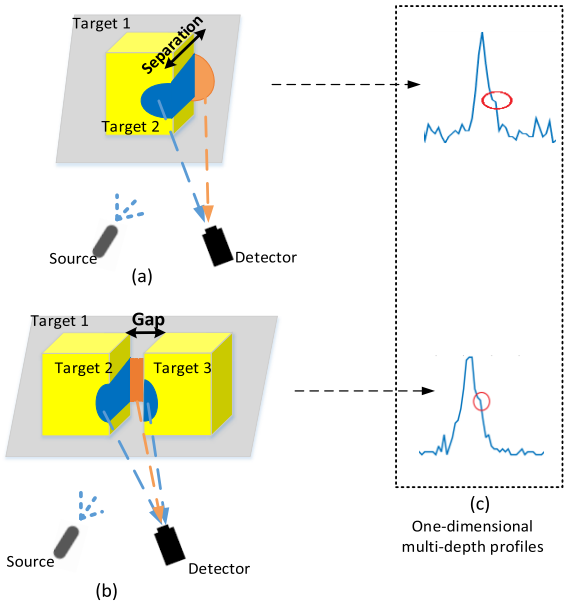

FIGURE 1. Examples of the PSSPC technique imaging scenes in which the scene response is a sum of responses from multiple reflectors. The orange dashed line is the reflection of the target 1. The blue dashed line is the reflection of the target 2 and target 3. (a) Imaging scene with two objects. (b) Imaging scene with three objects. (c) One-dimensional multi-depth profile.

range profiles simply by peak detection method. To sum up, the ability to accurately resolve multiple targets is limited by several factors, such as high flux of the noise photons, systematic transient distortions and complex patterns of light being reflected from targets. Hence, the imaging accuracy evaluated by Standard Deviation (STD) or Root Mean Square Error (RMSE) degrades. Different methods have been devised to analyze multiple light returns to overcome this problem. This is known as the problem of multi-depth recovery from full-waveform measurements [10]–[13].

Several full-waveform approaches in Ref [12] and in Ref [13] were proposed to interpret the photon detection data as samples from a distribution of the full-waveform observation. Although the STMCMC method shows 5 times faster than the RJMCMC method, it still takes 32s to reconstruct each range profile for the surface separation of 20cm [13]. It is difficult to bridge both the accuracy and the speed using such approaches.

Gao and NG [14] applied a blind deconvolution technique to recover the signal from the multiple scattering effects. In practice, Richardson–Lucy (RL) deconvolution is considered to be better than iterative blind deconvolution and has been proved to be robust and reliable to maintain the profile edge details [15], [16]. Joel F.*et al*. introduced the accelerated RL deconvolution to greatly enhance the resolution of the intensity modulated continuous wave (IM-CW) lidar [16]. However, RL deconvolution is known as better SNR but with the risk of amplifying noise [17]–[19]. According to this problem, Geert.*et al.* proposed Gauss pre-filtering RL algorithm [19].

In this letter, we solved the multi-depth imaging problem using pre-filtering accelerated RL deconvolution method (PARL) by transmitting pseudo-random bit-stream. Firstly, Anscombe transformation [20] and wavelet denoising were applied to the raw data as the pre-filtering stage. Then the accelerated RL deconvolution (ARL) method [15] was introduced to accurately recover the multi-depth profiles. As detailed in Section III, our framework was successful in accurately reconstructing the depth features of the square mounted on the flat board with varying separations. The separation RMSE has been reduced to 3.82 cm from one-dimensional range profiles for the surface separation of 8cm. The separation RMSE has been reduced to 3.2 cm for the surface separation of 10cm.The separation RMSE has been reduced to 2cm for the surface separation of 12cm. Finally, the proposed method is succeeded in recovering the image of the two squares, which are placed 0.5cm apart from each other and are both 8cm above the flat board. The average per pixel processing time of the proposed method is measured to be 0.01 seconds. The computation is carried out by Matlab and a computer with Intel(R) Core (TM) i7-7700HQ CPU @ 2.80 GHz.

II. THEORY

A linear system could be modeled by a set of linear integro-linear equations that correlates the system output to its input. Such a system may bring signal distortions when subjected to systematic transient distortions. Those distortions, often expressed as system impulse response (SIR), could be corrected by the deconvolution in Eq. (1).

$$R_{xy} = H \otimes f + B \tag{1}$$

where R_{xy} represents the Correlation Photon Distribution (CPD), which is calculated by correlating the reference sequence $x(n)$ and delayed versions of the transmitted sequence $y(n)$, depicted in Fig.2 (a). H denotes the SIR and f is referred to the recovered profile of targets. B indicates the correlated noise photons. $\otimes$ is the convolution operation. The target features to be recovered can be expressed as f, which is broadened by the convolution product of the detector impulse response and TDC impulse response.

The recovered target profile f here in the conventional RL method is given by

$$f_{k+1} = f_k \times \left(\frac{R_{xy}}{H \otimes f_k} * H\right) \tag{2}$$

where * indicates the correlation operation.

The acceleration method here we used is premised on vector extrapolation [15]. Our modified ARL algorithm PARL is given in Algorithm 1. The accelerated RL (ARL) method described in Ref [15] is originally used in gray-scale images restoration and is capable of achieving lower RMSE and fewer iterations than the conventional RL method. Despite this, it continues to encounter the problem of noise

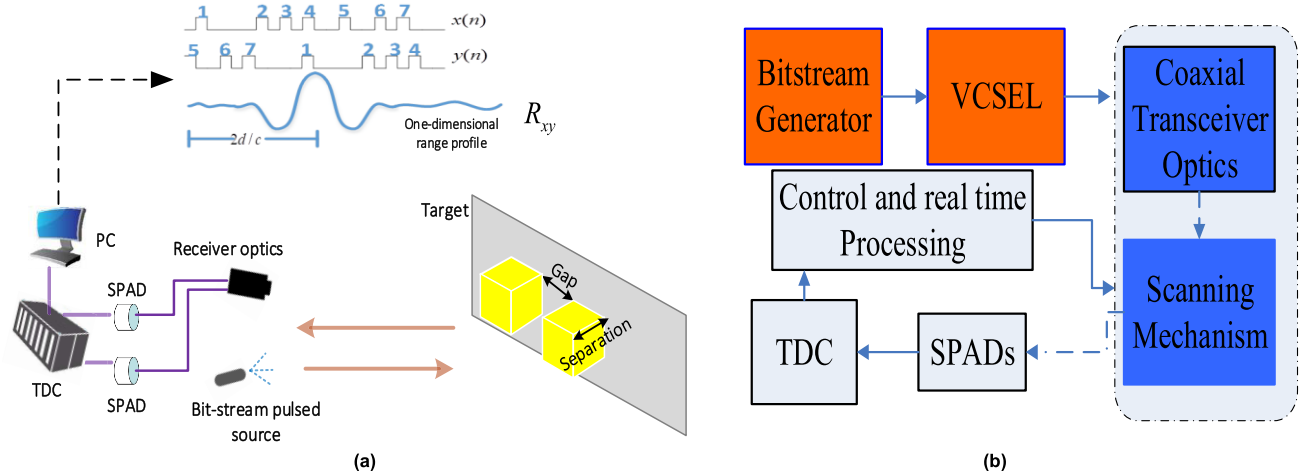

FIGURE 2. (a) 3D imaging principle. (Top) The principle of the correlation to obtain the one-dimensional range profile. (Bottom) A bit-stream pulsed optical source illuminates a pixel of the experimental scene that includes the squares and the flat board. The separation of the squares relative to the flat board varied from 6cm to 12cm. The gap between the two squares is variable from 0.5cm to 1.5cm. Each square has dimensions 3 cm × 3 cm. (b) Schematic diagram showing the key components of the imaging system. Two Single Photon Avalanche Diodes (SPADs) in connection with Time-to-Digital Converter (TDC) were used to detect two channels' photon stamps. The coaxial transceiver optics consist of the fiber coupler and the circulator. The two-dimensional rail with the movement range of 30cm×30cm was used as the scanning mechanism.

Algorithm 1 Pre-Filtering Accelerated RL Algorithm (PARL)

Input:	$R_{xy}, H, k, k_{\max}$
Output:	$\hat{x}^{(k)}$
Initialize:	R_{xy} is denoised to obtain noise-free data set R'_{xy}; $k = 1; \alpha_1 = \alpha_2 = 0; k_{\max} = 5; \hat{x}^{(0)} = R'_{xy}$
Repeat:	*While* $k \le k_{\max}$ $\hat{f}^{(k)} = \hat{x}^{(k-1)} \times (\frac{R'_{xy}}{H \otimes \hat{x}^{(k-1)}} * H)$; $df_k = \hat{f}^{(k)} - \hat{x}^{(k-1)}$; IF $k > 2$; $\alpha_k = \frac{\langle df_{k-1}, df_{k-2} \rangle}{\|df_{k-2}\|_2^2}$; End IF; $\hat{x}^{(k)} = \hat{f}^{(k)} + \alpha_k(\hat{f}^{(k)} - \hat{f}^{(k-1)})$; $k = k + 1$;

Algorithm 2 Correlation Deconvolution Imaging

Input:	R_{xy}, H, ε
Output	$\hat{x}_{opt}$

	1. Deconvolution: Obtain $\hat{x}_{opt}(i) : i \in [1, 2, \cdots, n]$ by the PARL.
	2. Hard thresholding: For $i = 1 : n$
	IF $\lvert\hat{x}_{opt}(i)\rvert < \varepsilon$
	$\hat{x}_{opt}(i) = 0$;
	End IF;
	End For;
	where ε is a small positive number.
	3. Depth averaging: Identify the two-time bins' indexes corresponding to two peaks of $\hat{x}_{opt}$ respectively and Replace each value by the center of mass method [21].

amplification. Unless modified to cope with noise, it is usually difficult to determine when to halt the iteration at all the pixels to prevent oscillations and divergence from the desired results by excessive acceleration.

In order to solve this problem, in this letter, prior to the deconvolution, the CPD data was denoised in three steps. First, the noise variance was stabilized by applying the Anscombe transformation. This step efficiently transforms Poisson noise into white Gaussian noise. Second, the magnitude of the noise was reduced by applying wavelet denoising using the MATLAB function wden with Coiflet wavelets of order 1. Third, an inverse transformation (Anscombe inverse exact unbiased transformation) was applied to obtain R'_{xy} as an estimate of the original noise-free data set. Then the ARL method was introduced to reconstruct the range profiles. Algorithm 2 is Correlation Deconvolution Imaging. After solving $\hat{x}_{opt}$ using Algorithm 1, we apply post-processing on $\hat{x}_{opt}$ that sets small residual nonzero elements to zero ($\varepsilon = 0.8$), detects two peaks by using the Matlab function findpeaks and averages closely-neighboring nonzero elements into a depth by the center of mass method (CM). This end-to-end processing is summarized in Algorithm 2.

The CM method described in Ref [21] is expressed as:

$$d_{CM} = \frac{\sum_{T \arg etbins} x(i)\tau(i)}{\sum_{T \arg etbins} x(i)} \tag{3}$$

where $\tau(i)$ is the time value corresponding to the i th index, $x(i)$ is the amplitude corresponding to the i th index.

The separation between two objects is given by:

$$\hat{d} = (d_{CM1} - d_{CM2}) \times \frac{c}{2} \tag{4}$$

where c is the speed of light.

Let $\hat{d}$ be the estimated separation at a pixel obtained by either the CM method or our proposed framework. $d_{actualseparation}$ is defined as the true distance between two separated targets. Then, the separation RMSE to quantify the recovery performance of the two-path signal over m measurements is expressed as:

$$RMSE = \frac{c}{2}\sqrt{\frac{1}{m}\sum_{n=1}^{m}(\hat{d}_n - d_{actualseparation})^2} \tag{5}$$

The separation RMSE is used to assess the imaging accuracy and to determine when to discontinue the PARL method. If $\overline{d}$ is defined as the average distance between two separated objects. Then, the separation STD is expressed as:

$$STD = \frac{c}{2}\sqrt{\frac{1}{m}\sum_{n=1}^{m}(\hat{d}_n - \overline{d})^2} \tag{6}$$

III. EXPERIMENT

A. SYSTEM IMPULSE RESPONSE

Figure 2 (b) shows a schematic diagram of our experimental imaging system using the PSSPC technique. Background light using an incandescent lamp was injected. An ANALOG DEVICE (ADI) series Vertical Cavity Surface Emitting Laser (VCSEL) with center wavelength of 850 nm was driven by 2.5GHz bit-stream as the illumination source. The bit-stream was in the form of m-sequence. Two SPADs in connection with a Pico Quant 300 TDC were used to detect two channels' photon stamps. The two SPADs are Perkin-Elmer commercial Single Photon Counting Modules with quantum efficiency $\eta = 0.45$, timing jitter less than 600ps, and dark counts less than 2×10^2 c/s. The Coaxial Transceiver Optics consist of the fiber coupler and the circulator. We observed that the diameter of the laser spot cast on a planar object at about 7 m distance was around 6.8 mm. The two-dimensional rail with the movement range of 30cm×30cm was used as the Scanning Mechanism.

In Ref [16], the SIR was derived from taking the theoretical Maximum Length (ML) sequence, autocorrelation function, then filtering it with a periodic Gaussian filter, regardless of the detector and other system components' transient distortions. In this letter, the SIR was measured by our system we presented in Fig.2 (b). Two fiber couplers were used. One of the two was used to transmit the light beam attenuated by fiber attenuators prior to being directly collected by the other fiber coupler. With the dark counts less than 2×10^2 c/s, two channels' time stamps were collected and correlated. By 50 measurements the average SIR was calculated and depicted in Fig.3.

The average SIR in Fig.3 is fitted by the Gauss fit method [22], [23]. The fitted SIR is about 1.4ns Full Width at Half-Maximum (FWHM), suggesting that 21cm surface-to-surface resolution can be achieved without using any signal processing [24]. In the presence of moderate noise and systematic transient distortions, two peaks may sometimes be partly or entirely overlapped and the peak separation is obscure. New signal processing methods should be introduced to improve the range resolution.

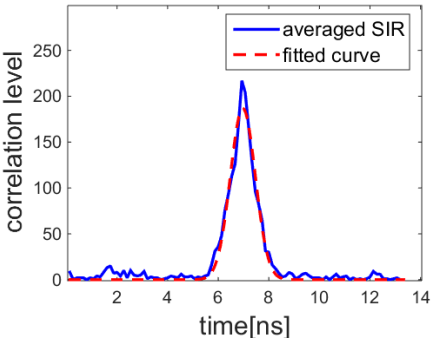

FIGURE 3. The averaged SIR (blue solid line) and the gauss fitted curve (red dashed line). An acquisition time of 0.004s was required and the dark counts were 200 c/s (counts per second).

B. ONE-DIMENSIONAL RANGE PROFILES RECOVERED WITH VARYING SEPARATIONS

To validate the multi-depth estimation of our proposed method, one of the two squares mounted on the flat board shown in Fig.2 (a) was used as one-dimensional experimental scene. The scene was positioned at a range about 7m from our system. The laser spot was projected on the depth boundaries of the two reflective objects: the square and the white flat board. The objects' reflection principle is shown in Fig.1 (a). The separation of the square from the flat board varies from 6cm to 12cm. Two channels' photon stamps were acquired within 0.004s dwell time. The photon counting rate was 1.5×10^6 c/s. An average of 6000 photon detections at each pixel were comprised of 600 noise photon counts and 5400 signal photon counts. Then the CPD was calculated.

After acquiring a particular scene's CPD, Algorithm 2 was applied. Besides, our initialization $\hat{x}^{(0)}$ was chosen to be R'_{xy} and the parameter ε was chosen to be 0.8. The H is set to be the average SIR we measured. The halting iteration number was chosen based on the minimum separation error. To illustrate the role played by the proposed method, Fig.4 (b), (e), (h) and (k) show the intermediate PARL output. According to the PARL output in Fig.4 (b), (e) and (h) from 10ns to 20ns, two peaks have been separated. After the hard thresholding, Fig.4 (c), (f), (i) and (l) show the output of Algorithm 2. The display range of x-axis in Fig.4 (c), (f), (i) and (l) is set from 8ns to 22ns. Each time bin's width is 0.4ns. It is observed that our proposed method is capable of resolving the separation of 6cm shown in Fig.4 (c). However, from Fig.4 (c), the estimated separation is 12.2cm by the depth averaging in Algorithm 2, which is considered an error of 6.2cm. Note that if the separation between the

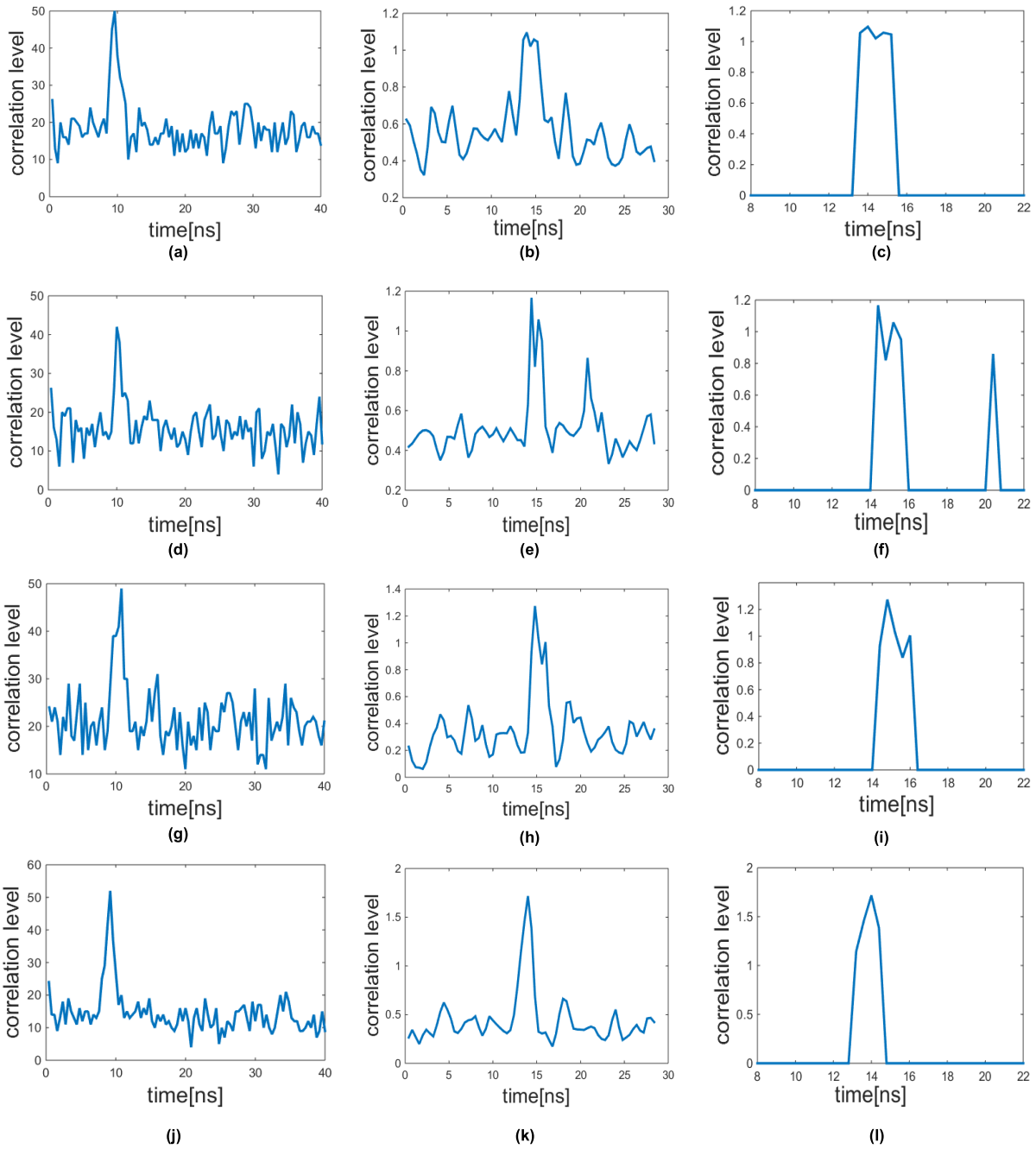

FIGURE 4. Three examples of raw CPD data collected from the square mounted on the flat board with variable separations of (a) 6cm, (d) 8cm and (g) 12cm. The solution of the PARL in Algorithm 1 for the surface separations of (b) 6cm, (e) 8cm and (h) 12cm. Note that the two peaks are separated and the extraneous background counts are reduced. The final result by Algorithm 2 for the surface separations of (c) 6cm, (f) 8cm and (i) 12cm. (j) The raw CPD data collected from the front side of the square. (k) One depth's reconstruction by PARL.(l) One depth's reconstruction by Algorithm 2.

square and the flat board is small (below 6cm), then our algorithm produces a large error towards the true separation. After the depth averaging, for the separations of 8cm [see Fig.4 (d)] and 12 cm [see Fig.4 (g)], the estimated separations are 9.5cm [see Fig.4 (f)] and 12.7cm [see Fig.4 (i)] respectively. The peak positions determined by the proposed method are shown to approach the true peak positions. Then the laser spot is projected on the front side of the square. It means that the light reflected from only one target contains a single depth. Fig.4 (l) shows the single-depth reconstruction by Algorithm 2.

With Algorithm 1, it is certain that there is an optimal solution along with the extension of the iteration number. Thus, in Fig.5, the statistical record with the 8 cm data set

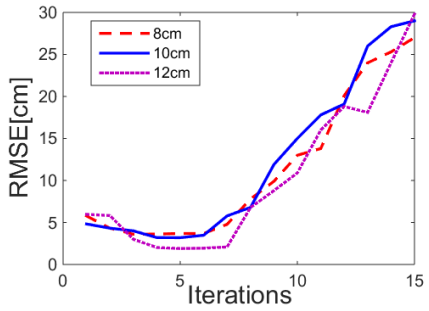

FIGURE 5. RMSE curves versus maximum number of iterations with variable separations of 8cm (dashed line),10cm (solid line) and 12cm (dotted line) by the proposed method.

(dashed line), 10cm data set (solid line) and 12cm data set (dotted line) about the setting of maximum number of iterations demonstrates the robustness of the proposed method. Here, the vertical axis represents the separation RMSE of 50 samples and the abscissa corresponds to the maximum number of iterations. The number of iterations at which the minimum RMSE is achieved depicted in Fig.5. Thus, we require an average of 5 PARL iterations ($k_{max} = 5$) per pixel.

The recovered range profiles in Fig.4 seem to demonstrate that the proposed method works. Then, to further explore the advantages of the proposed method, with the datasets in Table 1, the statistical record of 50 samples about the separation RMSE and the separation STD were made to evaluate the accuracy and stability of the results under the current settings. To illustrate the proposed method's advantage, the CM method is used to compare with Algorithm 2. Table 1 presents the statistical record of the proposed method and the CM method. As shown in Table 1, the separation STD has been improved more than the separation RMSE by the proposed method. For both algorithms, the RMSE and STD become larger as the separation becomes small. The CM method is a satisfactory approach for well-separated peaks; however, as the two surface return signals merge, the process becomes increasingly problematic. The larger error of depth separation estimated by the CM method is attributed to the inability to determine the time of flight accurately due to the superposition with the SIR and the fluctuation of background noise. Our proposed method successfully resolves the overlap peaks and outperforms the CM method, but it causes larger RMSE when the separation is 6cm shown in Table 1.

For the separation of 10cm, the solution of the proposed method demonstrates separation RMSE of 3.2cm and the CM method gives 15.02cm. The proposed method thus demonstrates an improvement in the separation RMSE by a factor of 4.7. With respect to the separation of 8cm, the solution of the proposed method demonstrates separation RMSE of 3.82cm and the CM method gives 15.4cm. The proposed method thus demonstrates an improvement in the separation RMSE by a factor of 4.

TABLE 1. Range statistical record of different separations.

	RMSE [cm]		STD [cm]	
Separation	Our method	CM	Our method	CM
6cm	18	24.5	4.69	24.1
8cm	3.82	15.4	2.75	14.6
10cm	3.2	15.02	1.87	13.9
12cm	2	9.5	0.47	4.08

C. TWO-DIMENSIONAL RANGE PROFILES RECOVERED WITH VARYING SEPARATIONS AND GAPS

To validate range resolution and accuracy, the object with 3 cm × 3 cm squares mounted on a flat board with varying separations and varying gaps was made [see Fig.2 (a)]. This test object was placed at a range about 7m and Algorithm 2 was applied. The scanning resolution was set to be 90 × 90. The minimum movement of the rail was set to 1mm. Fig.6 (a), (b) and (c) present the imaging result of the two squares with the gap of 1cm. In our 3D imaging system, fiber connections of the circulator, splitter and other fiber components increase the measured range. The measured range shown in Fig.6 is more than 7m. The separation of the squares from the flat board is 8cm [see Fig.6 (a)], 10cm [see Fig.6 (b)] and 12cm [see Fig.6 (c)]. It can be seen that the proposed method is succeeded in recovering useful depth features of the two squares. The color bar indicates the estimated depths of the objects. As the separation increases, the imaging of the two squares' boundaries becomes clear.

In Fig.6 (d) and (e), imaging squares' gap varies from 0.5cm [see Fig.6 (d)] to 1.5cm [see Fig.6 (e)]. The varied gap is used to test the lateral range resolution by the proposed method. The separation of the squares relative to the flat board is 8cm. From Fig.6 (d), we observe that our proposed multi-depth imager successfully distinguishes the two closely placed squares. Also, our proposed multi-depth imager distinguishes the squares from the flat board behind it, even though there exist mixed-depth pixels at boundaries and high background light plus dark counts. The narrow gap is possible to affect the scattered photons to produce more complex patterns of light. If the gap between the two squares is below 0.5cm, we almost fail to distinguish the two squares. Note that we calculate the separation RMSE, which is different from the true depth RMSE. Thus, the maximum depth subtracting the minimum depth on the color bar is larger than the separation RMSE indicated in Table.1. It implies that when calculating the separation RMSE, even the error is 0, the estimation results still remain deviation from the true depth, causing larger error shown in Fig.6

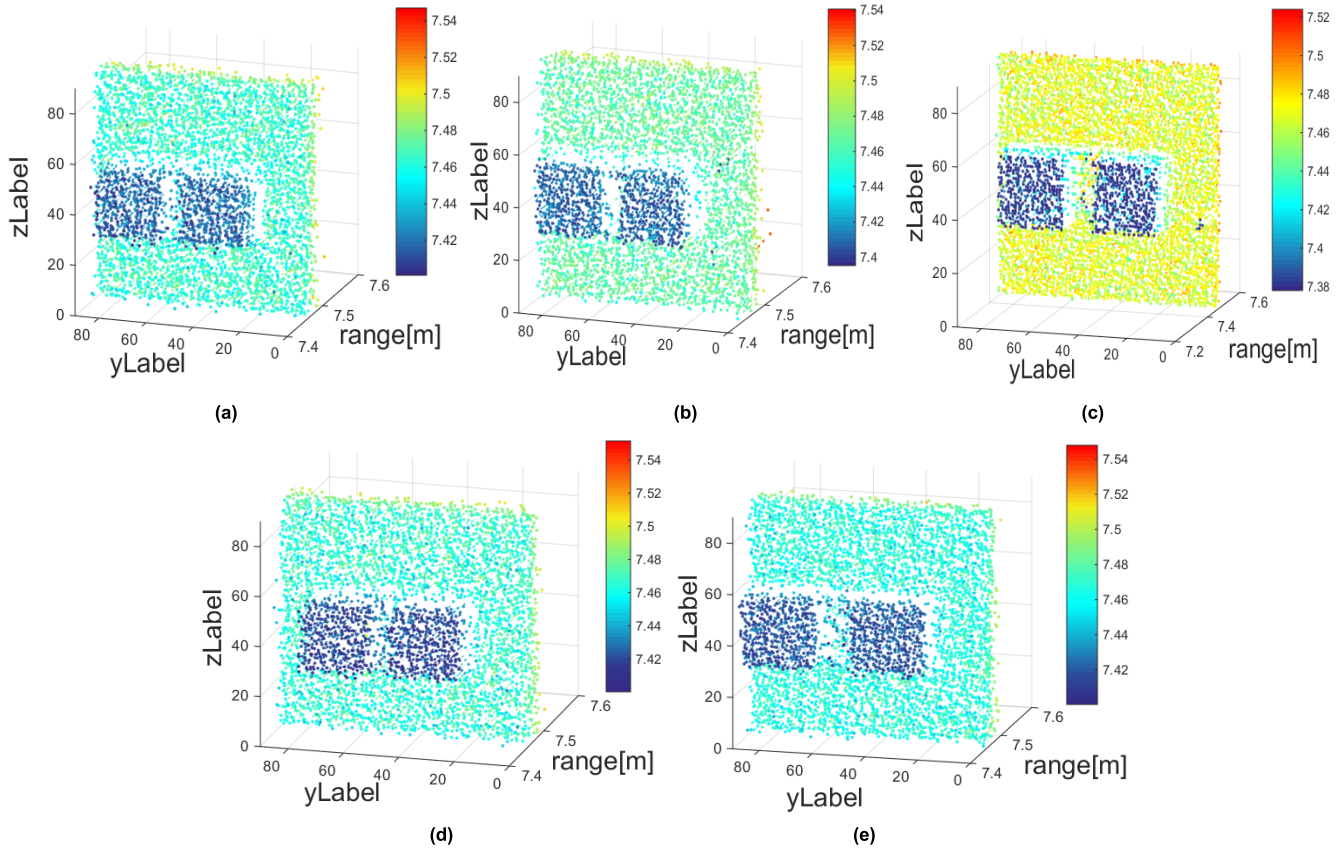

FIGURE 6. Three recovered images of the two separated squares for the separations of (a) 8cm, (b) 10cm and (c) 12cm by the proposed method. The images for varying gaps of (d) 0.5cm and (e) 1.5cm between the two squares.

IV. CONCLUSION

In this letter, sub-FWHM resolution by improving the range resolution from 21cm to 8cm has been successfully achieved based on PSSPC technique under low SNR condition. The proposed method gives an improvement in the separation RMSE by a factor of 4.7, compared to the conventional CM method, for the task of imaging a scene of two objects separated by a distance of 10cm. Besides, the proposed method has made an improvement in the separation RMSE by a factor of 4 for the surface separation of 8cm. Also, the proposed method has distinguished the two squares, which are closely placed 0.5cm apart from each other with the 6.8mm laser spot size. The proposed method is able to achieve sub-spot size lateral range resolution.

Our proposed algorithm is conducted with computational efficiency since we require an average of 5 PARL iterations per pixel. The post-processing step only requires a linear search over n bins. The CM method applied in Algorithm 2 only requires several bins' calculation as depicted in Fig.4 (c), (f), (i) and (l). When imaging the objects with 3 cm $\times$ 3 cm squares, the average per pixel processing time was measured to be 0.01 seconds and its total processing time was 81s with 90×90 pixel scans. This technique can achieve the lower RMSE and less calculation time in accurately recovering the two closely mounted squares. It provides a new prospect in recovering complex target profiles accurately by the PSSPC technique.

In the future work, it is of interest to study how to apply other post-processing methods with several signal photon counts per pixel. Also, techniques, such as range gating and narrowband optical filtering, can be incorporated to reject background counts at the data acquisition level to have a more accurate multi-depth reconstruction.

REFERENCES

[1] Q. Zhang, H. W. Soon, H. T. Tian, S. D. Fernando, Y. Ha, and N. Chen, "Pseudo-random single photon counting for time-resolved optical measurement," *Opt. Express*, vol. 16, no. 17, pp. 13233–13239, 2008.

[2] B. Büttgen, M.-A. E. Mechat, F. Lustenberger, and P. Seitz, "Pseudonoise optical modulation for real-time 3-D imaging with minimum interference," *IEEE Trans. Circuits Syst. I, Reg. Papers*, vol. 54, no. 10, pp. 2109–2119, Oct. 2007.

[3] B. Büttgen, T. Oggier, M. Lehmann, R. Kaufmann, S. Neukom, M. Richter, M. Schweizer, D. Beyeler, R. Cook, C. Gimkiewicz, C. Urban, P. Metzler, P. Seitz, and F. Lustenberger, "High-speed and high-sensitive demodulation pixel for 3D imaging," *Proc. SPIE.*, vol. 6056, Jan. 2006, Art. no. 605603.

[4] Y. Zhang, Y. He, F. Yang, Y. Luo, and W. Chen, "Three-dimensional imaging lidar system based on high speed pseudorandom modulation and photon counting," *Chin. Opt. Lett.*, vol. 14, Nov. 2016, Art. no. 111101.

[5] S. Shen, Q. Chen, W. He, and Y. Wang, "Boundary evaluation and error correction on pseudo-random spread spectrum photon counting system," *Chin. Opt. Lett.*, vol. 15, no. 9, Sep. 2017, Art. no. 090101.

[6] M.-C. Amann, T. M. Bosch, M. Lescure, R. A. Myllyla, and M. Rioux, "Laser ranging: A critical review of unusual techniques for distance measurement," *Proc. SPIE*, vol. 40, no. 1, pp. 10–19, Jan. 2001.
[7] P. A. Hiskett, C. S. Parry, A. McCarthy, and G. S. Buller, "A photon-counting time-of-flight ranging technique developed for the avoidance of range ambiguity at gigahertz clock rates," *Opt. Express*, vol. 16, no. 18, pp. 13684–13691, Sep. 2008.
[8] T. F. Refaat, S. Ismail, M. N. Abedin, S. M. Spuler, S. D. Mayor, and U. N. Singh, "Lidar backscatter signal recovery from phototransistor systematic effect by deconvolution," *Appl. Opt.*, vol. 47, no. 29, pp. 5281–5288, Oct. 2008.
[9] X. Ai, R. Nock, J. G. Rarity, and N. Dahnoun, "High-resolution random-modulation CW lidar," *Appl. Opt.*, vol. 50, no. 22, pp. 4478–4488, 2011.
[10] J. Castorena, C. D. Creusere, and D. Voelz, "Using finite moment rate of innovation for LIDAR waveform complexity estimation," in *Proc. 44th Conf. Rec Asilomar Conf. Signals Syst. Comput.*, vol. 50, Nov. 2010, pp. 608–612.
[11] J. Castorena and C. D. Creusere, "Compressive sampling of LIDAR: Full-waveforms as signals of finite rate of innovation," in *Proc. 20th Eur. Signal Process. Conf.*, vol. 34, Aug. 2012, pp. 984–988.
[12] P. J. Green and A. Mira, "Delayed rejection in reversible jump Metropolis–Hastings," *Biometrika*, vol. 88, no. 4, pp. 1035–1053, Dec. 2001.
[13] W. Yin, W. He, G. Gu, and Q. Chen, "Approach for LIDAR signals with multiple returns," *Appl. Opt.*, vol. 53, no. 30, pp. 6963–6969, 2014.
[14] J. L. Gao and C. N. Ng, "Deconvolution filtering of ground-based LIDAR returns from tropospheric aerosols," *Appl. Phys. B.*, vol. 76, no. 5, pp. 587–592, May 2003.
[15] D. S. C. Biggs and M. Andrews, "Acceleration of iterative image restoration algorithms," *Appl. Opt.*, vol. 36, no. 8, pp. 1766–1775, Mar. 1997.
[16] J. F. Campbell, B. Lin, A. R. Nehrir, F. W. Harrison, and M. D. Obland, " Super-resolution technique for CW lidar using Fourier transform reordering and Richardson–Lucy deconvolution," *Opt. Lett.*, vol. 39, no. 24, pp. 6981–6984, 2014.
[17] G. Gong, H. Zhang, and M. Yao, "Construction model for total variation regularization parameter," *Opt. Express*, vol. 22, no. 9, pp. 10500–10508, 2014.
[18] R. L. White, "Image restoration using the damped richardson-lucy method," *Proc. SPIE*, vol. 2198, pp. 1342–1348, Jun. 1994.
[19] G. Kempen, L. J. V. Vliet, and P. Verveer, "A quantitative comparison of image restoration methods for confocal microscopy," *J. Microsc.*, vol. 185, no. 3, pp. 354–365, Mar. 1997.
[20] M. Diop and K. S. Lawrence, "Deconvolution method for recovering the photon time-of-flight distribution from time-resolved measurements," *Opt. Lett.*, vol. 37, no. 12, pp. 2358–2360, Jun. 2012.
[21] M. S. Oh, H. J. Kong, T. H. Kim, K. H. Hong, and B. W. Kim, "Reduction of range walk error in direct detection laser radar using a geiger mode avalanche photodiode," *Opt. Commun.*, vol. 283, no. 2, pp. 304–308, Jan. 2010.
[22] M. J. Stevens, R. H. Hadfield, R. E. Schwall, S. W. Nam, and R. P. Mirin, "Fast lifetime measurements of infrared emitters using a low-jitter superconducting single-photon detector," *Appl. Phys. Lett.*, vol. 89, Jul. 2006, Art. no. 031109.
[23] O. Steinvall and T. Chevalier, "Range accuracy and resolution for laser radars," *Proc. SPIE.*, vol. 5988, Oct. 2005, Art. no. 598808.
[24] T. Neimert-Andersson, "3D imaging using time-correlated single photon counting," Ph.D. dissertation, Dept. Eng. Sci., Univ. UPPSALA, Uppsala, Sweden, 2010.

SHEN SHANSHAN received the B.S. degree in electronic engineering in China, in 2007, and the master's degree in signal and information processing from the School of Electronic Engineering and Optoelectronic Techniques, Nanjing University of Science and Technology, where she is currently pursuing the Ph.D. degree in optical engineering. She has been teaching for more than ten years in the Zijin College, Nanjing University of Science and Technology. She is also an Associate Professor. Her research interests include three-dimensional reconstruction and laser ranging based on TCSPC technique.

CHEN QIAN received the M.S. and Ph.D. degrees from the School of Electronic Engineering and Optoelectronic Techniques, Nanjing University of Science and Technology. He is currently a Professor with the Department of Optoelectronic Engineering and also the Vice President of the Nanjing University of Science and Technology. He has led many research projects and authored more than 100 journal articles. His research interests include real-time digital image processing, optoelectronic imaging, electro-optical displaying technology, optoelectronic signal processing, and transmission.

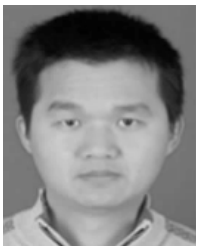

HE WEI JI received the M.S. and Ph.D. degrees from the School of Electronic Engineering and Optoelectronic Techniques, Nanjing University of Science and Technology. He is currently a Professor with the Jiangsu Key Laboratory of Spectral Imaging and Intelligence Sense. His research interests include optoelectronic imaging, electro-optical displaying technology, and optoelectronic signal processing.

GU GUO HUA received the B.S. and Ph.D. degrees from the School of Electronic Engineering and Optoelectronic Techniques, Nanjing University of Science and Technology. He is currently a Professor with the Jiangsu Key Laboratory of Spectral Imaging and Intelligence Sense. His research interest includes optoelectronic imaging.